The nonlinear evolution of two surface quasi-geostrophic vortices

Xavier Carton, Jean N Reinaud, Armand Vic, Jonathan Gula

Geophysical and Astrophysical Fluid Dynamics
Vol. 00, No. 00, 00 Month 2023, 1–17

The nonlinear evolution of two surface quasi-geostrophic vortices

Xavier Carton †*, Jean N. Reinaud ‡, Armand Vic † and Jonathan Gula (IUF member) †
† LOPS/IUEM/UBO, Brest, France
‡ School of Mathematics and Statistics, University of St Andrews, UK.
(*Received 00 Month 20xx; final version received 00 Month 20xx*)

Using a numerical model of the two-level surface quasi-geostrophic equations, we investigate the evolution of two circular temperature patches, one located at each level. We vary the vortex intensities, radii, and the vertical distance between the two levels. We also study different radial profiles of temperature for each vortex. This paper considers two main situations: (initially columnar) vortices with like-signed buoyancies which are linearly unstable and may break, and initially tilted vortices with opposite-signed buoyancies, which may align vertically. Numerical experiments show that (1) identical contra-rotating vortices break into hetons when initially perturbed by low azimuthal modes; (2) asymmetric vortices stabilise nonlinearly more often and can form quasi-steady baroclinic tripoles; (3) co-rotating vortices can align when the two fluid levels are close to each other vertically, and when the vortices are initially distant from one another by less than three radii; (4) for initially more distant vortices, the two vortices rotate around the plane center; (5) in all cases, the vortex contours are disturbed by Rossby waves. These results compare favorably to earlier results with internal quasi-geostrophic models, but apply more easily to near surface dynamics in the ocean. Further modelling efforts may extend the present study to fully three dimensional ocean dynamics.

Keywords: Two-level model, surface quasi-geostrophy, vortex stability, Burger number, modal analysis

1. Introduction

Vortices are long-lived oceanic flow structures, with a mostly horizontal circulation imposed by the Earth's rotation and the density stratification (Carton 2001). Vortices play a substantial role in the transfer of water masses, heat and momentum across the oceans (Richardson 1983, McWilliams 1991, Provenzale 1999, Gula *et al.* 2019). They can last from a few weeks to a few years and drift over distances as large as half an ocean basin (Carton 2010). The robustness of oceanic vortices, also called "eddies", is related to their internal balance between the pressure and velocity field, over large radii (several tens of kilometers) and thicknesses (several hundreds of meters) van Heijst (2010). The radial pressure anomaly balancing the circular motion is related to an internal density anomaly (Hopfinger and van Heijst 1993). Indeed, oceanic vortices trap and carry heterogeneous water masses, characteristic of their regions of formation, far away from these regions (Robinson 2012, Gula *et al.* 2022).

Insofar as the hydrostatic and geostrophic balances mostly hold inside these vortices, the quasi-geostrophic (QG) model is an appropriate framework to describe their dynamics and evolution (Reinaud *et al.* 2022). Nevertheless, due to the ocean's density stratification, more than one layer, or vertical level, is necessary in this model to adequately represent these vortices (Reinaud 2019). The simplest model available to describe oceanic vortices is the two-layer, quasi-geostrophic model (Flierl 1978). This model represents two slabs of homogeneous water, with different densities, superimposed, and interacting via their density interface. In each layer the velocity is mostly horizontal and geostrophic, and the dynamics is governed by the evolution of layerwise potential vorticity with forcing and dissipation (Charney 1948). This two-layer quasi-geostrophic model has been the framework of the study of baroclinic

*Corresponding author:xcarton@univ-brest.fr

instability of parallel flows by Phillips (Phillips 1954) and of baroclinic vortex instability (Sokolovskiy and Verron 2013, Flierl 1988, Carton and McWilliams 1996, Carton *et al.* 2010).

In the presence of buoyancy anomalies concentrated vertically over a shallow depth, the quasi-geostrophic model can be expressed via the evolution of buoyancy (or temperature) anomalies, which are the singular equivalents of potential vorticity. This restriction of the general QG model is the surface quasi-geostrophic model (SQG) which represents the advection of buoyancy anomalies on the upper or lower surfaces of the ocean (Bretherton 1966, Held *et al.* 1995, Lapeyre 2017, Smith and Bernard 2013). The SQG model has been used mostly in a one-level configuration for vortex and turbulence studies (Carton 2009, Carton *et al.* 2011, Tulloch and Smith 2009, Lapeyre and Klein 2006, Klein *et al.* 2008, Harvey and Ambaum 2011, Harvey *et al.* 2011, Badin and Poulin 2019). A SQG model coupled with an internal quasi-geostrophic model has also been used for the study of coupled surface flow-internal vortex Perrot *et al.* (2010), Reinaud *et al.* (2016, 2017a,b).

Recently, the present authors have investigated the linear stability of a circular vortex in a two-level, SQG model (Vic *et al.* 2022), comprising both surface and bottom buoyancy anomalies. The aim of the present work is to extend the linear study of two-level vortices to their nonlinear dynamics, that is, investigate the possible formation of hetons, or of more complex vortex compounds, from these two-level vortices (e.g. Gryanik (1983), Hogg and M. (1985a,b)). For two like-signed buoyancy anomalies, one on each surface, we assess the finite-amplitude evolution of monochromatic angular perturbations, and the possibility of vortex breaking, or of topological rearrangement of the initial vortices. The structure and regularity, or not, of the final vortex compound cannot be assessed from the linear analysis previously carried out. This is why we resort here to numerical modelling. We also extend our previous study to parameter regimes which are not accessible to linear analysis, for the sake of simplicity and of tractability of the analytical solutions.

This paper is organized as follows: we present the SQG model equations, initial conditions and numerical implementation in section 2. In section 3, we address the nonlinear interaction of two initially perturbed, like-signed temperature anomalies. These anomalies are initially aligned vertically. We assess the influence of various physical parameters on the nonlinear evolution of these unstable vortices. In section 4, we consider the case of two circular, opposite-signed, temperature anomalies, initially offset horizontally from each other. We study their possible vertical alignment. A discussion on the stability of these two-level SQG vortices follows. Finally, conclusions are drawn from the study in section 4.1.

2. Physical and numerical model

2.1. *Model equations and initial conditions; physical parameters*

2.1.1. *Model equations*

In the ocean, pressure can be decomposed into a static part (corresponding to the ocean at rest) $\bar{p}$ and a dynamic part (related to motion) p'. The former is in hydrostatic balance with the static density $d\bar{p}/dz = -\bar{\rho}g$ and the latter term can be in hydrostatic balance with the dynamical part of density $\partial p'/\partial z = -\rho' g$. This balance will hold in our study.

In the quasi-geostrophic model, the Coriolis acceleration mostly balances the horizontal pressure gradient (the relative acceleration is weak) so that the horizontal velocity is essentially non-divergent. Then the dynamic pressure is related to a streamfunction ψ via $\psi = p'/\rho_0 f_0$, where $f_0 = 2\Omega \sin(\lambda)$ is the local Coriolis parameter (Ω being the Earth rotation rate and λ the latitude). The dynamic density is also related to the streamfunction via $b = -g\rho'/\rho_0 = f_0 \partial\psi/\partial z$, where b is the buoyancy, and ρ_0 is a reference density. Note that the linear equation of state for seawater is $\rho = \rho_0[1 - \alpha(T - T_0)]$, in the absence of salinity variation; then the

dynamic density anomaly is related to the temperature anomaly via $\rho' = -\rho_0 \alpha T'$ (α is the thermal dilatation coefficient and T_0 is a temperature reference). Therefore $b = g\alpha T'$ and, within a constant ratio, buoyancy and temperature anomalies are equivalent.

The equation governing the quasi-geostrophic model in the bulk of the ocean, is the conservation of potential vorticity q in the absence of forcing and of dissipation:

$$dq/dt = \partial q/\partial t + J(\psi, q) = 0, \quad z \in (-H, 0),$$

where $J(f, g)$ is the horizontal Jacobian operator and H is the depth of the ocean. The quasi-geostrophic potential vorticity is

$$q = \partial^2\psi/\partial x^2 + \partial^2\psi/\partial y^2 + \ (\partial/\partial z)[(f_0^2/N^2)(\partial\psi/\partial z)],$$

where N is the Brunt Väisälä frequency (the static stability frequency).

When the potential vorticity is zero in the bulk of the ocean but is concentrated at the surface and at the bottom ($q = q_1\delta(z = 0) + q_2\delta(z = -H)$), the potential vorticity equation becomes an equation for buoyancy evolution on these two surfaces (Bretherton 1966):

$$db/dt = \partial b/\partial t + J(\psi, b) = 0, \quad z = 0, -H. \tag{1}$$

This is the two-level surface quasi-geostrophic (SQG) model, with

$$b = f_0\partial\psi/\partial z \ \text{ and } \quad \mathrm{q} = 0.$$

Assuming that the fluid domain is horizontally unbounded, the buoyancy and the streamfunction can be written as

$$b(x, y, z = 0, t) = \int\int b_1(k, l, t) \ \exp(i[kx + ly])\, dk\, dl,$$

$$b(x, y, z = -H, t) = \int\int b_2(k, l, t) \ \exp(i[kx + ly])\, dk\, dl,$$

$$\psi(x, y, z, t) = \int\int A_{kl}(t) \ \phi_{kl}(z) \ \exp(i[kx + ly])\, dk\, dl,$$

where k, l are the horizontal wavenumbers, b_1, b_2 the upper and lower buoyancies, and A_{kl}, ϕ_{kl} the associated Fourier coefficients. When the Brunt Väisälä frequency is constant ($N = N_0$), the condition of zero potential vorticity int the bulk of the ocean leads to

$$d^2\phi_{kl}/dz^2 - (K^2N_0^2/f_0^2) \ \phi_{kl} = 0,$$

where $K^2 = k^2+l^2$. Normalizing buoyancy by f_0, we have $b = \partial\psi/\partial z$; then, the streamfunction at the two levels is

$$\psi(x, y, z = 0, t) = \int\int \psi_1(k, l, t) \ \exp(i[kx + ly])\, dk\, dl, \tag{2}$$

$$\psi(x, y, z = -H, t) = \int\int \psi_2(k, l, t) \ \exp(i[kx + ly])\, dk\, dl, \tag{3}$$

where

$$\psi_1(k, l, t) = b_1(k, l, t)/[K \tanh(KH)] - b_2(k, l, t)/[K \sinh(KH)],$$

$$\psi_2(k, l, t) = b_1(k, l, t)/[K \sinh(KH)] - b_2(k, l, t)/[K \tanh(KH)].$$

Equation (1) allows us to march b_1, b_2 in time, and these fields can then be inverted into the streamfunction using equations (2) and (3).

2.1.2. *Initial conditions and aim of the simulations*

Our two-level SQG model is initialized with a single disk of uniform buoyancy at each level. The corresponding streamfunction is given in (Vic *et al.* 2022). Here, we consider the interaction of two vortices with like-signed buoyancy in section 3 and with opposite-signed buoyancy in section 4. Any axisymmetric distribution of buoyancy corresponds to a steady state. Hence in the present case, the pair of circular, co-axial, vortices is steady. In section 3, to study the stability of these vortices, we perturb their bounding contour (the rim of the disk) with a monochromatic perturbation in angle, with azimuthal mode m. Using a numerical model of the two-level SQG equations, we study the nonlinear evolution of the perturbed vortex. In particular, we assess whether the vortices break, and/or, rearrange as new types of vortices such as dipoles or tripoles. In section 4, we set the two vortices on each side of the center of the plane and we study their vertical re-alignment with respect to the horizontal offset and to the vertical distance between the SQG levels.

2.1.3. *Physical parameters*

In this study, the vortex radii R_1, R_2, the buoyancies B_1, B_2, the deformation radius $R_d = NH/f_0$ and the azimuthal mode m are the physical parameters under consideration. One value of buoyancy and the deformation radius can be used to scale time and lengths. Therefore, the independent (dimensionless) physical parameters are: B_2/B_1, R_2/R_1, R_1/R_d and m.

Due to the large number of parameters, we first investigate a reference case, for which the first two parameters are set to 1, and then we perform a sensitivity study of the instability to the independent physical parameters by varying them separately.

2.2. *Numerical model*

Our numerical model is a pseudo-spectral model with 256×256 collocation points to determine the nonlinear regimes (or 512×512 points for higher resolution when specified). Equations are marched in time with a mixed Euler-Leapfrog scheme (an Euler step every 50 time steps). The spatial derivatives are calculated in Fourier space and FFT's are used to transform the fields from physical to Fourier space and back. The domain size is $4\pi \times 4\pi$ (except for a few simulations of vortex alignment, when the vortices are initially distant from each other; then the domain size is $8\pi \times 8\pi$). Very weak viscosity is used (biharmonic diffusion) with $\nu_4 = 8\ 10^{-7}$ at 256-resolution and $\nu_4 = 5\ 10^{-9}$ at 512-resolution. The numerical model has been validated in a previous study of vortex merger Oulhen *et al.* (2022).

To assess the validity of our results, we also compare them with those of a CASL (contour advection semi Lagrangian) code often used in the literature for SQG vortex dynamics (Reinaud *et al.* 2016, 2017b,a). Though biharmonic diffusion is weak, the spectral model is more dissipative than the CASL model. The spectral code tends to slightly spread out the buoyancy contours while the CASL code produces more small vortex fragments. Nevertheless, an extensive comparison of the two codes over many cases shows that they lead to similar results when these small fragments are finally dissipated: the main vortices form similar aggregates in both model results. Here, we present only the results of the spectral code.

3. Nonlinear evolution of linearly unstable SQG vortices with like-signed temperature anomalies

In the literature, studies have shown that baroclinically unstable vortices in two-layer quasi-geostrophic flows (with finite internal potential vorticity) could evolve nonlinearly into hetons (Hogg and M. 1985a,b, Reinaud and Carton 2009b), contra-rotating ellipses (Carton and McWilliams 1996) or in baroclinic tripoles (Reinaud and Carton 2009a, Sokolovskiy and Car-

ton 2010). Such nonlinear evolutions are also observed in two-layer ageostrophic shallow-water flows (Baey and Carton 2002). Here, we study the various nonlinear regimes of linearly unstable, two-level SQG vortices, with various values of B_2/B_1, R_2/R_1, R_1/R_d and of the azimuthal mode of deformation m.

3.1. *Vortices with equal radii and intensity*

3.1.1. *Sensitivity of nonlinear regimes to the vortex size/deformation radius*

Firstly, we set $B_2/B_1 = 1$, $R_2/R_1 = 1$, and we run several simulations, varying R_1/R_d for the elliptical mode of deformation $m = 2$.

For $R_1/R_d = 1$ or 1.25, the vortices elongate elliptically in each layer and eventually break into two hetons. This is also the case for baroclinically unstable vortices in the two-layer(internal) quasi-geostrophic model (Helfrich and Send 1988). For $R_1/R_d = 1.67$, this hetonic evolution is followed by their splitting. For $R_1/R_d = 2$, the vortices break over a mixed azimuthal mode 2 and 4 (with a complex elliptical and square deformation) leading to several fragments. For $R_1/R_d = 2.5$, azimuthal mode 4 now prevails and the vortices break into four hetons. Finally, for $R_1/R_d = 5$, azimuthal mode 6 is dominant in the unstable vortex evolution.

Clearly, higher modes of deformation become more unstable as the two levels get closer to each other vertically. This is related to the link between the horizontal and vertical scales in the SQG model (this link is due to the vanishing potential vorticity). Short horizontal scales have a short vertical reach. As the two vortices get closer vertically, their small scale perturbations can interact more efficiently. This is consistent also with the linear analysis of instability published previously (Vic *et al.* 2022).

We have also run several simulations, with the same values of B_2/B_1, R_2/R_1 varying R_1/R_d for the triangular mode of deformation $m = 3$. For $R_1/R_d = 1$, the azimuthal mode 2 is the most unstable perturbation and the vortices break into two hetons. For $R_1/R_d = 2$, mode 3 is now more unstable, and in the nonlinear evolution, the vortices from three hetons. For $R_1/R_d = 5$, the vortex breaks on a mode 8. This confirms the growth in wavenumber of the most unstable wave as R_1/R_d increases. The destabilization of short waves as R_1/R_d increases has also been noticed for the baroclinic instability of vortices in two-layer quasi-geostrophic models (Flierl 1988, Helfrich and Send 1988).

Note that this conclusion also holds for vortices with a smoother radial profile, like the parabolic profile of buoyancy, detailed in the appendix, or a top-hat profile in relative vorticity; we observe also the same nonlinear regimes using the CASL code instead of our spectral model. Therefore this conclusion is generic.

3.1.2. *Study of the hetonic evolution of the unstable vortices*

Now, we investigate in more detail the case $B_2/B_1 = 1$, $R_2/R_1 = 1$, $R_1/R_d = 1$, $m = 2$. This is our reference case. In figure 1, we present the time evolution of buoyancy at each level The two vortices evolves regularly and simultaneously at the two levels from near disks to ellipses. During their evolution, the angle between them increases to reach approximatively $/pi/4$ and does not vary substantially afterwards. The aspect ratio $\lambda = b/a \leq 1$ of the ellipses decreases. Here b and a are the major and minor semi-axis lengths respectively. Further in time, the vortices evolve towards a peanut shape. This shape indicates the presence of higher azimuthal modes of deformation, in particular mode $m = 4$ which is the first harmonic of the fundamental perturbation ($m = 2$). The strongly deformed vortices finally break at their center and give birth to two baroclinic vortex pairs, called hetons (Flierl 1988, Helfrich and Send 1988).

A Fourier analysis of the azimuthal modes at each level is performed. Results are shown in figure 2. Clearly, the elliptical components of the deformation grow first, followed in time and

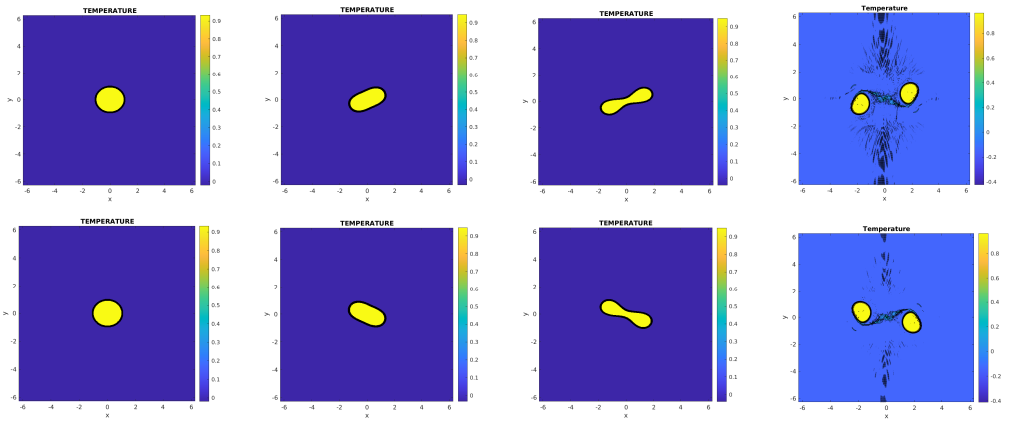

Figure 1. Hetonic breaking of an unstable two-level SQG vortex with uniform buoyancy ; time-series of horizontal maps of buoyancy; the parameters are $B_2/B_1 = 1$, $R_2/R_1 = 1$, $R_1/R_d = 1$, $m = 2$. The upper row shows the upper level buoyancy, and the lower row, the lower level one. Times shown are $0, 8, 12, 20$ model time units.

in amplitude by the $m = 4$ mode. The antisymmetric mode $m = 1$ and the triangular mode $m = 3$ always have a small amplitude.

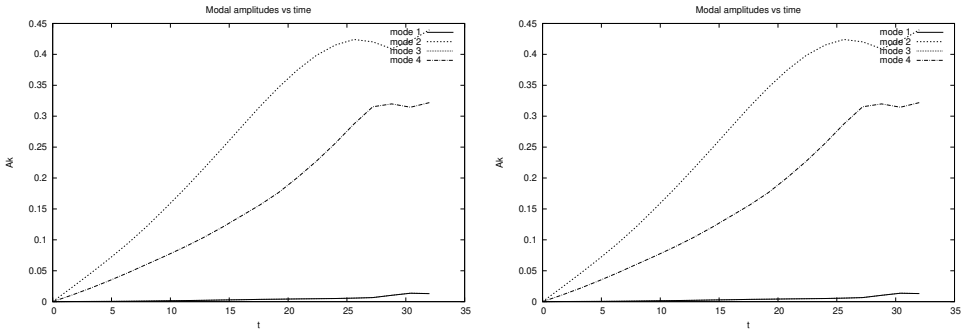

Figure 2. Fourier analysis of hetonic breaking of the unstable two-level SQG vortex with uniform buoyancy ; the parameters are $B_2/B_1 = 1$, $R_2/R_1 = 1$, $R_1/R_d = 1$, $m = 2$. The various azimuthal modes shown are $m = 1$, 2, 3, 4. Left panel: upper level; right panel: lower level.

The ellipticity and the angle of each vortex are calculated from the geometric moments of buoyancy (not shown here for brevity). The value obtained for the relative angle between the two vortices is $\pi/4$. This relative orientation of the two vortices maximises the destabilizing influence exerted by each vortex on the other (or, in other words, it maximizes the resonance of unstable Rossby waves on the vortex contours). It must also be noted that the two vortices become irreversibly deformed (they acquire the peanut shape) when their aspect ratio is smaller than 0.25. This critical value is reminiscent of that necessary for the breaking of the Kirchoff elliptical vortex in two-dimensional incompressible fluids ($\lambda = 0.33$).

3.1.3. *A vortex evolution model with a single ellipse or with two-level ellipses*

Considering the similarity between the evolution of our unstable circular vortices, and the evolution of strongly elongated Kirchhoff ellipses, we study now the stationarity and the stability of an elliptical vortex of constant buoyancy with respect to its initial aspect ratio.

First, we perform numerical simulations with a single level SQG model (the buoyancy being confined to a surface, over an infinitely deep ocean/fluid). Specifically, we run simulations for $a/b = 1/\lambda = 3, 4, 5$. Two simulations are run for each case: a short one with a high-frequency temporal sampling to determine the initial rotation rate Ω of the ellipses, and a long one to assess the long-term evolution of each ellipse.

We numerically obtain an estimate for Ω for a unit-buoyancy elliptical vortex in the range

$3 \leq a/b \leq 5$: $\Omega \approx \lambda$. Note that the rotation rate of an elliptical vortex with a parabolic profile of buoyancy has been computed in (Dritschel 2011) (the streamfunction associated with a parabolic profile of buoyancy is given here in appendix). This latter paper shows that indeed Ω is linear in λ in the range $\lambda \in [0, 0.3]$.

Then, we observe that the constant buoyancy elliptical vortex with $\lambda = 1/3$ (or with $\lambda = 1/4$) elongates to a peanut shape but finally shrinks back to an ellipse. On the contrary, an elliptical SQG vortex initially with $\lambda = 1/5$ elongates irreversibly to a peanut-shaped vortex and then breaks into two separate vortices (two dipoles). Again, this indicates that higher modes can grow on an elliptical vortex, during its unsteady, and possibly unstable, evolution; this confirms our Fourier analysis of the unstable circular vortex, presented above.

Figure 3 shows the time series of buoyancy for the ellipse with aspect ratio 1/5. The growth of mode $m = 4$ is clear in the deformation of the ellipse. The growth of this mode, simultaneous with that of mode $m = 2$ is confirmed by a Fourier analysis of the elliptical vortex in time. This Fourier analysis computes the increase of the modal perturbations from their initial (non-zero) values (i.e. the initial ellipse is subtracted from the instantaneous vortex shape). As a conclusion of single ellipse simulations, the critical aspect ratio for elliptical SQG vortex

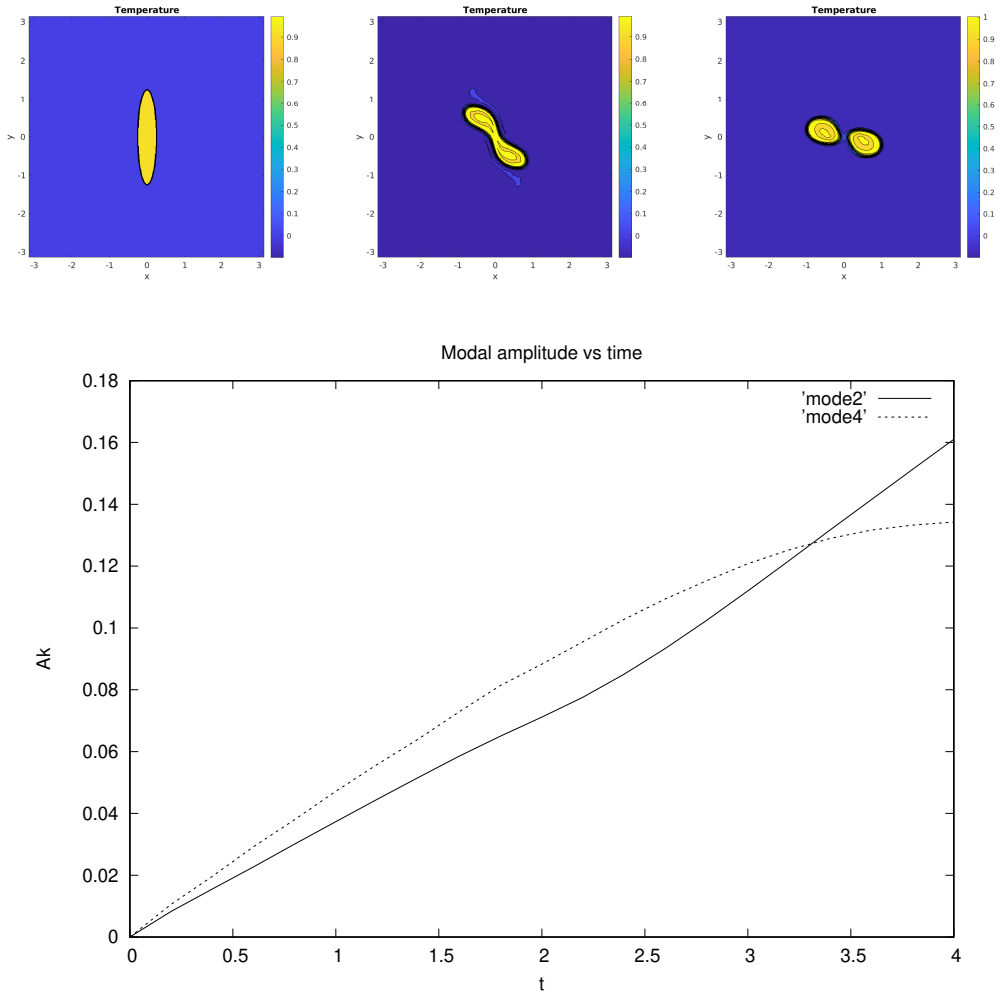

Figure 3. Top : Time series of horizontal maps of buoyancy showing the nonlinear breaking of an elliptical vortex, with uniform buoyancy, in a vertically semi infinite fluid; the aspect ratio of the ellipse is $b/a = 1/5$ initially. Times shown are $t = 0$, 4, 8. Bottom " Fourier analysis of the one-level SQG ellipse with uniform buoyancy. The two azimuthal modes shown are $m = 2$, 4. For $m = 2$ the initial value was subtracted.

breaking (with constant buoyancy) lies in $\lambda \in [0.2, 0.25]$. Nevertheless, in our vortex instability

simulations (subsection 3.1.2), the upper level vortex is not isolated from the lower level one. Therefore, now we perform simulations with identical ellipses of constant buoyancy at the two levels (with the same buoyancy, same size, same aspect ratio).

For $R_d = 1$, the elliptical vortices do not break and they eventually evolve to adopt a steady elliptical shape, for $\lambda > 0.2$ as in the one-layer case. For $R_d = 0.8$, ellipses with aspect ratios larger than 0.3 are meta-stable and oscillate around a peanut shape (see panel 2 of figure 3). On the contrary, for $R_d = 0.6$, the ellipse breaks for a large range of aspect ratios $\lambda \in [0.3, 0.8]$, because as H or R_d decreases, mode $m = 4$ becomes more unstable linearly thus favoring vortex breaking (Vic *et al.* 2022).

3.2. *Vortices with different radii or intensities*

We next vary the vortex parameters and we seek to classify and explain their unstable evolutions in these cases. Figure 4 describes the various nonlinear regimes obtained when varying R_2/R_1 and B_2/B_1, for $R_d/R_1 = 1$ ($H = 1$) and $m = 2$. In the linear analysis of our previous paper (Vic *et al.* 2022), R_2/R_1 was not varied to keep tractable algebraic equations. Clearly,

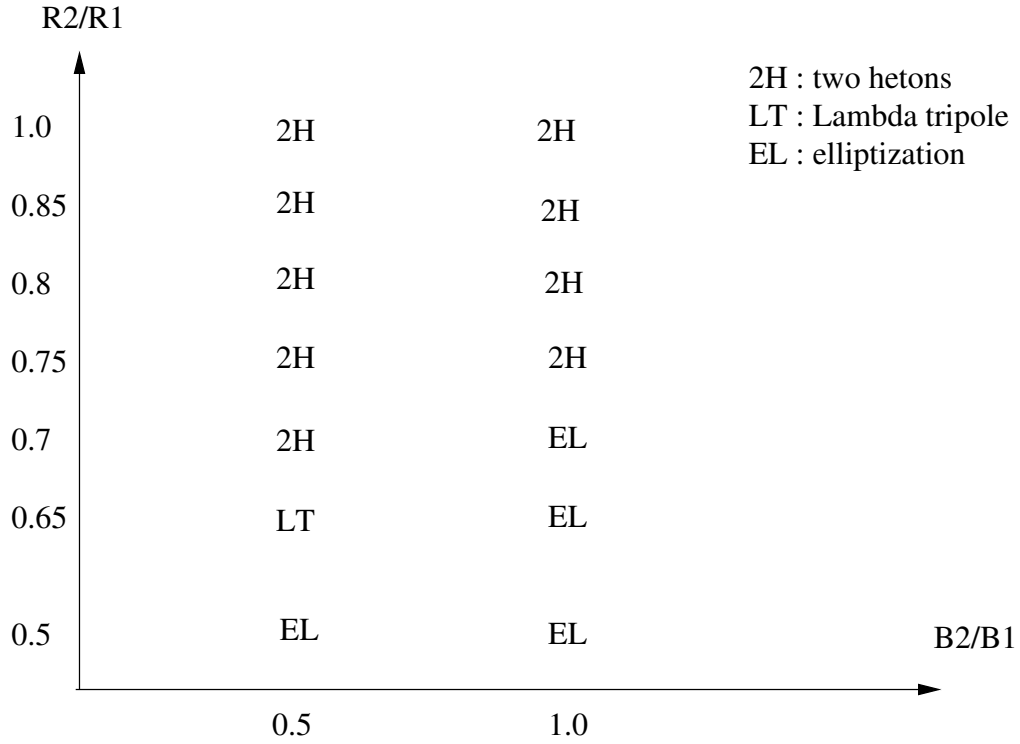

Figure 4. Nonlinear regimes of the unstable two-level Eady vortex, with respect to their radii and buoyancies, for $B_1 = 1$, $R_1 = 1$, $R_2 = R_d$ ($H = 1$), $m = 2$.

the linearly unstable vortex breaks into two hetons when the vortex radii are identical at both vertical levels. When the lower vortex is smaller and less intense (and therefore has a smaller influence on the upper level vortex than the upper level vortex has on it), the lower level vortex breaks into two symmetric vortices, on each side (horizontally) of the upper level vortex. This evolution is much slower than that leading to the formation of two hetons. Here, after nonlinear stabilization, the vortex compound thus obtained is called a Λ-tripole, a structure observed previously, in particular in the collision of two oppositely-signed hetons (Reinaud and Carton 2009a, Sokolovskiy and Carton 2010); the formation of a Λ-tripole is illustrated in figure 5. This figure presents a time-series of horizontal maps of buoyancy, at the upper and lower levels, for this evolution. In this case, the upper vortex undergoes a strong elongation

which the lower vortex breaks into two symmetric parts. After several turn-over periods of the whole structure, the upper level vortex ellipticity relaxes to a smaller value while the lower two vortices become its satellites on each side. The whole structure rotates and its ellipticity continues to oscillate, due to the weak dissipation used in the simulation.

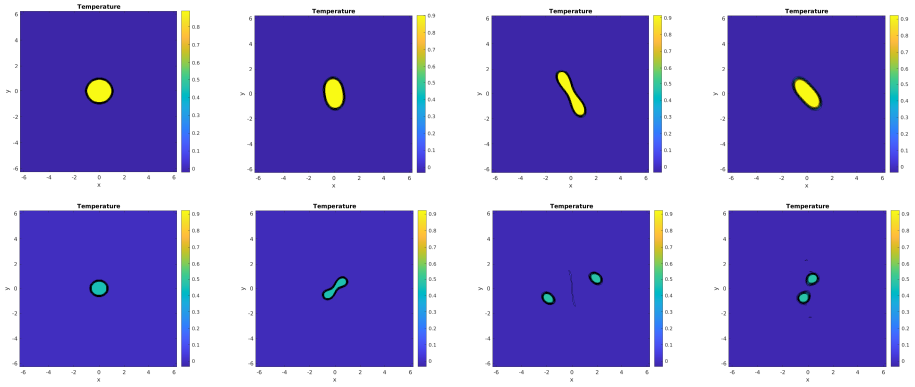

Figure 5. Λ-tripole formation from the nonlinear evolution of an unstable two-level SQG vortex with uniform buoyancy ; time-series of horizontal maps of buoyancy; the parameters are $B_2/B_1 = 0.5$, $R_2/R_1 = 0.65$, $R_1/R_d = 1$, $m = 2$. The upper row shows the upper level buoyancy, and the lower row, the lower level one. Times shown are 0, 48, 72, 120 model time units.

The Fourier analysis of the various azimuthal modes for this case, is shown on figure 6. We can note that again, only the even modes grow significantly. In the upper layer, mode $m = 2$ grows with superimposed oscillations, a result of the contra-rotation of the two-ellipses (such an oscillation is also show in (Carton and McWilliams 1996) Mode $m = 4$ grows more slowly but follows the general trend of mode $m = 2$. Both modal amplitudes reach a peak after which they stabilize, decay and oscillate. The maximal deformation corresponds to the third panel of figure 5 where the vortex is very elongated. The last stage (stabilisation) corresponds to the relaxation of the vortex towards an ellipse in the upper layer and to two satellites in the lower layer. Note that the lower layer perturbation amplitude is weaker, but that it acts on a weaker vortex. This lower layer vortex breaks earlier in the evolution of the whole structure. When the two vortices have similar buoyancies, but with a smaller lower

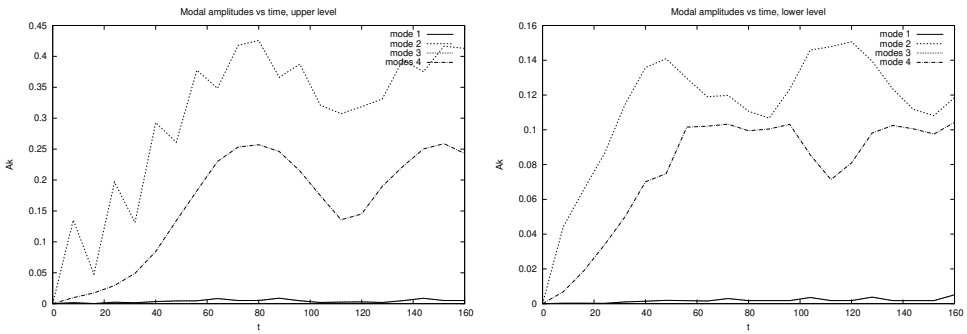

Figure 6. Fourier analysis of the unstable two-level SQG vortex forming a Λ-tripole; the parameters are $B_2/B_1 = 1$, $R_2/R_1 = 1$, $R_1/R_d = 1$, $m = 2$. The various azimuthal modes shown are $m = 1, 2, 3, 4$. Left panel: upper level; right panel: lower level.

vortex, their mutual deformation can become insufficient to break them as hetons. The final outcome of the instability is two contra-rotating elliptical vortices at the two levels (Carton and McWilliams 1996). The formation of contra-rotating ellipses is illustrated in figure 7. This figure presents the upper and lower level maps of buoyancy in the case $R1 = 0.5\,R2$, $B1 = B2$, $m = 2$, $R_1 = R_d$. Clearly the vortex ellipticity increases at each level while the vortex

rotates. The periodic shear exerted by each vortex on the other level vortex leads to a pulsating aspect ratio. The lower level vortex, which is smaller, is more deformed.

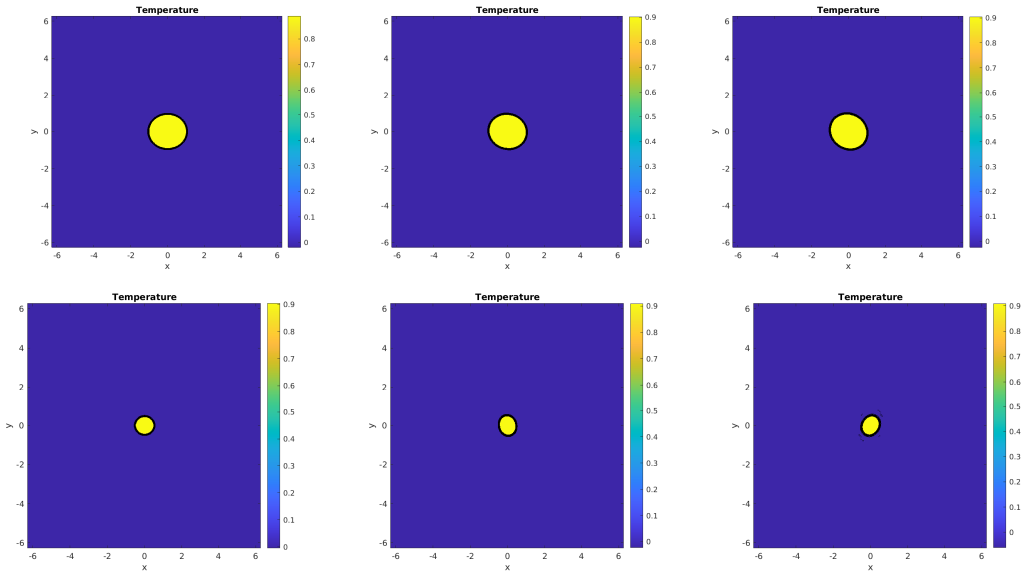

Figure 7. Nonlinear evolution of an unstable two-level SQG vortex with uniform buoyancy in a disk; the parameters are $B_2/B_1 = 1$, $R_2/R_1 = 0.5$, $R_1/R_d = 1$, $m = 2$. The upper row shows the upper level buoyancy, and the lower row, the lower level one. Times shown are $0, 90, 180$ model time units.

When varying R_2/R_1 and B_2/B_1, for $H = 0.5$ and $m = 2$, higher modes grow and in particular, when the elliptical mode $m = 2$ is perturbed, its harmonic $m = 4$ grows on the vortex. Both modes are unstable, even if the graver mode is slightly more unstable. Therefore, the final outcome of the nonlinear simulation is usually two hetons, a Λ-tripole or an ellipse, with smaller features due to the growth of mode 4 (see figure 8).

Further simulations are performed varying R_1/R_d and B_2/B_1 for $R_1 = R_2$ and $m = 2$. They show the growth of mode $m = 4$ for $R_d = 0.4$, 0.5 and of mode $m = 6$ for $R_d = 0.2$ in agreement with the linear stability analysis of (Vic *et al.* 2022). Simulations are also performed with an initial perturbation of mode $m = 3$. They show the breaking of the unstable vortex into hetons for $R_d = 1$, into Λ-tripoles for $R_d = 0.5$ and vortex breaking on short unstable waves $m = 6$, 8 for $R_d = 0.2$. Again, this confirms the pre-eminence of short waves for small H.

3.3. *A model of the Λ-tripole with three vortices on two levels*

We shwo here that an initial aggregate of three vortices, one at the center of the upper level, two laterally shifted at the lower level, can adjust nonlinearly to a Λ-tripole. We run a simulation with $B_1 = 1, B_2 = 0.5$, $R_1 = 1, R - 2 = 0.5$, $H = R_d = 1$, $d = 4R_2$ starting from three circular vortices. Figure 9 shows that each vortex deforms under the influence of the other two vortices, and in particular, elongates. The upper level vortex finally adjsts as an ellipse. The lower level satellite vortices then lie along the upper level vortex boundary.

4. Evolution of two offset SQG vortices, with opposite-signed temperature anomalies

In this section, we assess the robustness of a two-level SQG vortex, with opposite-signed temperature anomalies vertically. More specifically, we study the ability of an initially tilted

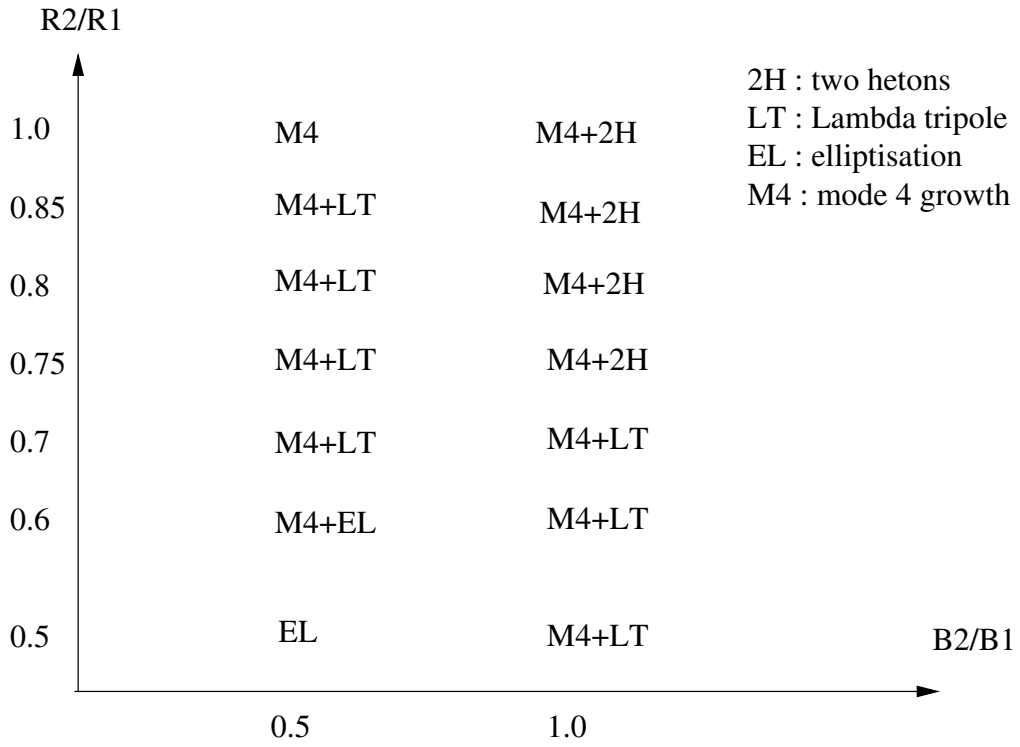

Figure 8. Nonlinear regimes of the unstable two-level Eady vortex, with respect to their radii and buoyancies, for $B_1 = 1$, $R_1 = 1$, $R_1 = 2R_d$ ($H = 0.5$), $m = 2$.

vortex to straighten up. In the ocean or in the atmosphere, drifting vortices are affected by a perturbation with horizontal mode $m = 1$. This perturbation leads to the tilting of the vortex with respect to the vertical axis. Again, we consider vortices with uniform buoyancy, that we offset horizontally by an initial distance d.

Figure 10 shows the various evolutions of tilted vortices for $R_2/R_1 = 1$, $B_2/B_1 = 1$, with respect to H (which is also R_d/R_1) and to d/R. The nonlinear evolutions are either towards the vertical re-alignement of the vortices, or their co-rotation around a central axis with little or no convergence towards the center.

For $H \leq 1.0$, alignment occurs for vortices initially distant of 3.3 radii. When vortices are initially farther away, the simply rotate around the center of the plane. Note that this critical distance $d/R = 3.3$ is close to the critical distance for the merger of two vortices, with uniform vorticity, in two-dimensional incompressible flows (Melander *et al.* 1988). It is also the critical distance for the merger of two vortices in a two-layer (internal) quasi-geostrophic model, when the vortices are confined in the upper layer (Polvani *et al.* 1989). When H is increase beyond 1, the critical distance for alignment decreases rapidly. For $H = 1.25$ it lies below 3. For $H = 1.4$, no complete alignment is observed any more. Only a moderate convergence of the two vortices occurs. Their distance decreases by half and then oscillates.The vortices mostly co-rotate. For $H = 1.5$, only a weak convergence followed by a weak radial oscillation, accompanies the co-rotation of the two vortices. Finally, for $H \geq 2$, only co-rotation is observed.

Note the partial similarity with the alignment diagram for two-layer, internal, quasi-geostrophic vortices, presented in figure 7 of (Polvani 1991). The critical value for alignment is also $d/R \approx 3.3$ and the maximal value of $1/\gamma$ (the equivalent of H in our study) is unity. Note also that, for very weak d/R initially, alignment is replaced by partial convergence.

The final state of the vortex depends on H. Various cases are shown below.
Firstly, for $B_1 = 1, B_2 = -1.0$, $R_1 = R_2 = 1.0$, $H = R_d = 1$, $d = 1$, alignment occurs. Figure 11 shows time series of buoyancy maps. the two vortices overlap more with time. To ensure

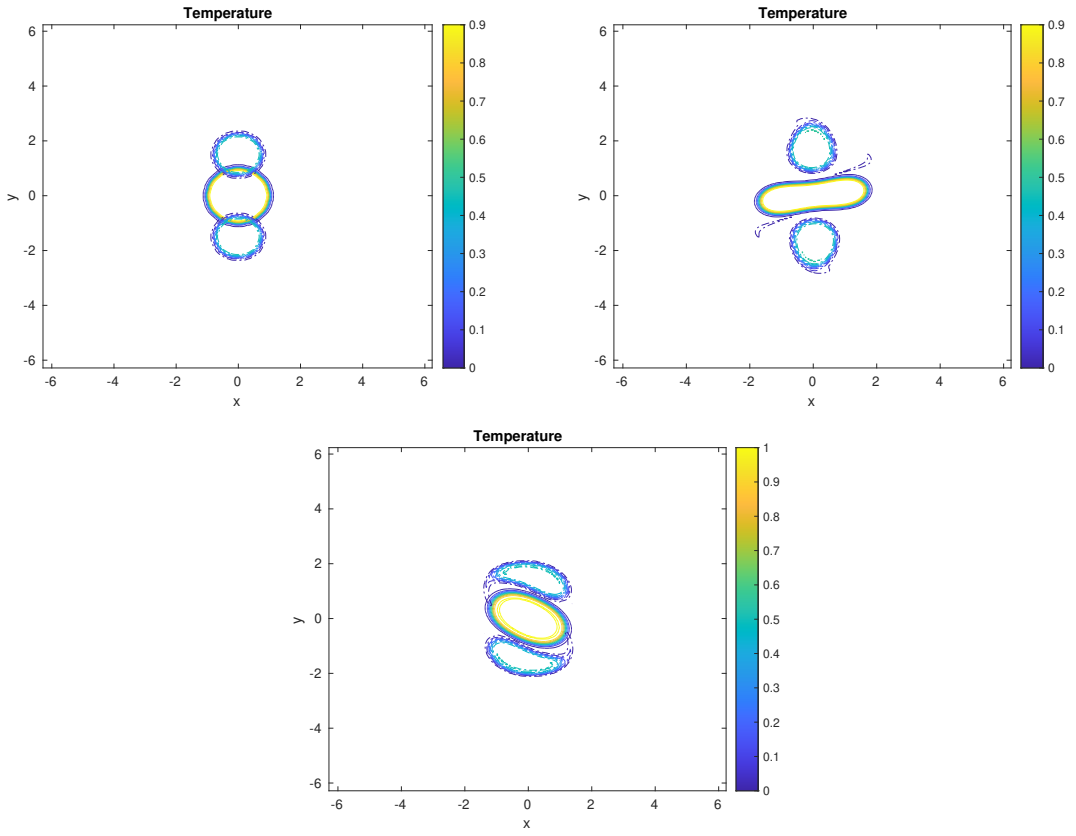

Figure 9. Time series of buoyancy maps for the upper level (solid lines) and the lower level (dashed lines) superimposed, showing the evolution of a vortex aggregate towards a Lambda tripole. Times shown are t=0, 28, 42 model time units. The vortex parameters are $B_1 = 1, B_2 = 0.5$, $R_1 = 1, R - 2 = 0.5$, $H = R_d = 1$, $d = 4R_2$

conservation of angular momentum, they shed filaments which are wrapped around the final vortex. The interaction of the central vortex with the peripheral vorticity supports vortex contour waves (vortex Rossby waves) which induce an phase shift between the two vortices. This explains why the inter-centroid distance oscillates while decreasing with time.

The following figure (12) shows that initially the streamlines and the buoyancy isocontours do not coincide (the upper level is shown here; the situation is symmetric at the lower level). This indicates that the buoyancy field is unsteady and that buoyancy will be advected towards the center of the plane (as shown by the streamlines). At the final time of the simulation (same figure), the buoyancy distribution is not yet steady but the streamlines match the buoyancy contours better. A longer simulation would be necessary to attain full stationarity, if any.

On the contrary, for $B_1 = 1, B_2 = -1.0$, $R_1 = R_2 = 1.0$, $H = R_d = 1$, $d = 4$, co-rotation occurs. Figure 13 shows time series of buoyancy maps. Clearly, each vortex rotates around the center of the plane, as shown by the inter-centroid distance, which varies little. The mutual influence of the two vortices is manifested by the Rossby waves on the vortex boundaries. As it appears in this figure, low modes of deformation grow first (modes 1 and 2, leading to a slightly asymetric ellipse for the vortex contours). Then higher modes grow by nonlinear interaction: this is seen on the last plot where a square (mode 4) deformation of the vortices appears. Nevertheless, this contour deformation never leads the vortices to deform so much to join near the center of the plane. Vertical alignment does not occur.

Finally, the regimes of weak to moderate convergence, with oscillation, lie in between the previous two regimes. The time variation of the intercentroid distance increases from co-rotation, to weak to moderate convergence and finally to vertical alignment. The amplitude of contour deformation also increases. The two joint effects favor alignement.

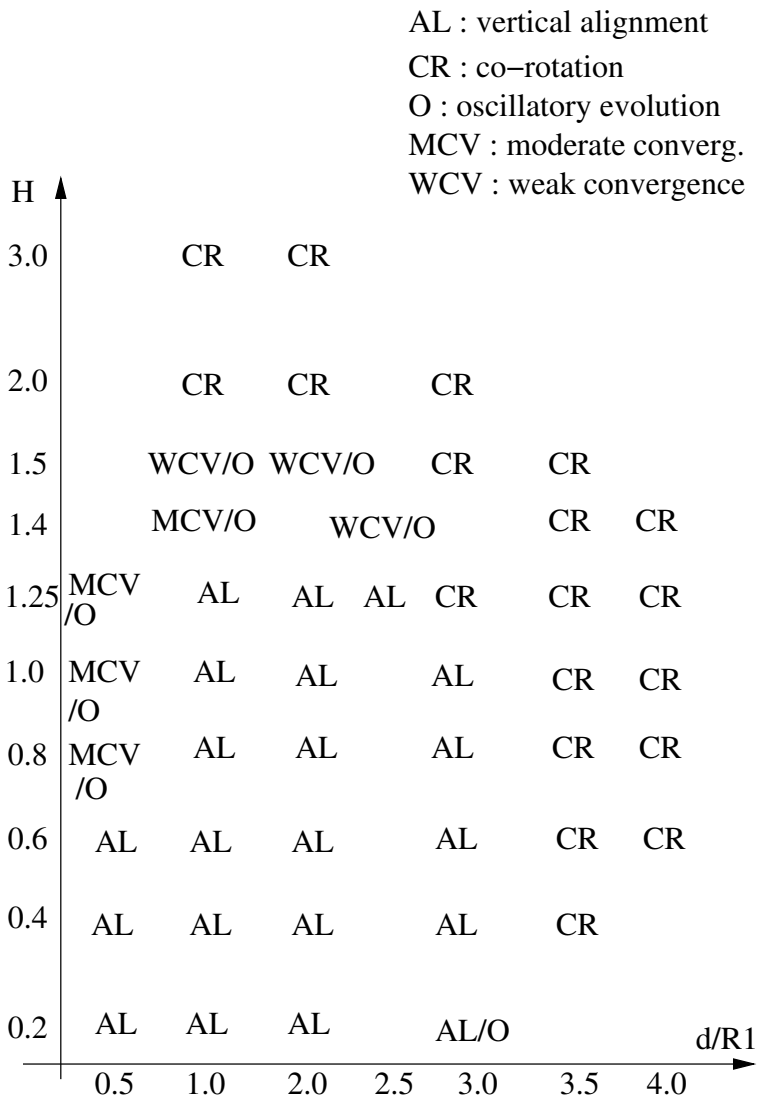

Figure 10. Nonlinear regimes of the tilted two-level Eady vortex, with respect to the vertical height of the domain H (or R_d/R_1) and to d/R_1 for $R_1 = R_2 = 1$ and $B_1 = B_2 = 1$. A indicates a vertical alignment of the two vortices, while CR denotes the co-rotation of the two vortices, with no or little decrease of their mutual distance.

4.1. *Discussion*

Our numerical experiments yielded the following results:

- for like-signed buoyancies at the upper and lower level (contra-rotating vortices), baroclinic instability can grow for increasing azimuthal wavenumbers as the fluid height decreases. Low mode ($m = 2, 3$) perturbations lead to hetonic breaking when the two vortices have comparable size and strength. On the contrary, for asymmetric vortices, vortex elliptisation or the formation of Λ-tripoles, are observed.
- Clearly, the formation of a Λ-tripole results from a nonlinear equilibration of the linearly unstable vortex. Higher modes of perturbation saturate at finite amplitude, in particular mode $m = 4$. It was also shown that a Λ-tripole is an attractor for nearby states: three vortices initialised in this configuration, but with a circular shape, deform until they reach the configuration observed in the nonlinear experiments of baroclinic vortex instability.
- For opposite-signed buoyancies at the upper and lower level (co-rotating vortices), vertical alignment can occur when the total height of the fluid is smaller than, or equal to

unity, and when the initial distance between the two vortices is smaller than, or equal to, three radii. Unequal vortices have not been considered here.
- In both the alignment and the co-rotation regimes, vortex Rossby waves are observed. In the alignment regime, they participate in the overlapping of buoyancy in time, and to the appearance of a mode 1 deformation (corresponding to a dipolar effect), finally leading to the convergence of vortices near the center of the plane.
- Intermediate regimes, between the former two, exist, exhibiting radial oscillations at various degrees. They occur more specifically for larger fluid heights (vertically more distant buoyancy levels).

These results comfirm and extend those previously obtained with a two-layer (internal) quasi-geostrophic model: in particular for baroclinic vortex instability (Flierl 1988, Helfrich and Send 1988). Clear analogies exist in the nonlinear evolutions, in particular the existence of nonlinearly equilibrated states for linearly unstable vortices, or the possible breaking of linearly unstable vortices into hetons. Similarly, previous studies found that vortices with like-signed potential vorticity could align in a two-layer quasi-geostrophic model if the vortices were large and close enough initially (Polvani 1991). These similarities can be related to the similarity between the Phillips and Eady models of baroclinic instability of jets (Eady 1949, Phillips 1954). Nevertheless, the SQg model produces more fine-scale features (filaments) and also leads to higher vertical velocities Lapeyre (2017). This is important in particular for near surface dynamics. Note that Smith and Bernard (Smith and Bernard 2013) noted that the SQG model can apply to a depth with a rapid change in stratification. This is the case of the base of the oceanic mixed layer. Therefore, our study pertains to surface intensified oceanic vortices, that is, vortices intensified in the upper 200- 400m of the ocean. The internal quasi-geostrophic model, on the contrary, pertains to deeper vortices. Despite this, results from the two models concerning the baroclinic instability of vortices, or their ability to align vertically, are quite similar.

4.2. *Conclusion*

The present results extend the previous results obtained with internal quasi-geostrophic dynamics, but they should be extended to ageostrophic dynamics (either in a two-level SQG^{+1} model or in a fully stratified, primitive equation, model). Oceanic vortices have complex vertical structures, and, when deformed, they are associated with finite vertical velocities, Such three-dimensional motions are not included in the present study, and will modify our results, via the inclusion of high frequency components of velocity.
Concerning observations at sea, new measurement devices (tow-yo, gliders) allow repeated measurements of interacting vortices at the submesoscale (McWilliams 1985, Chavanne *et al.* 2010, Bosse *et al.* 2016). Very high resolution numerical models also show evidence of such processes (Gula *et al.* 2015, Morvan *et al.* 2019). Such interactions were proved to strengthen these small vortices against the decay due to ambient shear and strain effects, turbulent diffusion, Rossby wave dispersion or topographic interactions, and thus make submesoscale eddies more robust. In particular it is important to quantify the efficiency of vortex alignment and vortex merger, in three-dimensional ocean dynamics, when the vortices are not isolated. Such a quantification will refine assessments of the contribution of oceanic eddies to heat and salt transport at large-scale.

Appendix A:

Here we calculate the streamfunction associated with a parabolic radial distribution of buoyancy for a two-level SQG vortex

$$B^s = B_0^s\sqrt{1-r^2}\ He(1-r) \qquad B^b = B_0^b\sqrt{1-r^2}\ He(1-r) \tag{A.1}$$

where He is the Heaviside function. The angular velocity of a single vortex defined by this steady state is drawn in Figure A2

Indeed, for any buoyancy b^s or b^b :

$$\psi^s(r,\phi,z=0,t) = \sum_{n\in N}\int_0^\infty \frac{J_n(\rho r)}{\sigma\sinh(\rho\sigma)}\left(\widehat{b^b} - \widehat{b^s}\cosh(\rho\sigma)\right)\mathrm{d}\rho\ e^{in\phi},$$

$$\psi^b(r,\phi,z=1,t) = \sum_{n\in N}\int_0^\infty \frac{J_n(\rho r)}{\sigma\sinh(\rho\sigma)}\left(\widehat{b^b}\cosh(\rho\sigma) - \widehat{b^s}\right)\mathrm{d}\rho\ e^{in\phi}. \tag{A.2}$$

where $\sigma = N_0H/f_0$ N_0 the Brunt-Vaisala frequency, f_0 the Coriolis frequency, and H the thickness of the fluid layer.

Computing the streamfunction of the steady state requires the Fourier transforms of the steady state buoyancies : for $\rho > 0$ and $n \in Z^*$:

$$\widehat{B^s}(\rho,n) = \frac{B_0^s}{2\pi}\int_0^{2\pi}\int_0^1 \sqrt{1-r^2}\ J_n(\rho r)r\mathrm{e}^{-in\phi}\ \mathrm{d}r\ \mathrm{d}\phi = 0 \tag{A.3}$$

For $n = 0$, posing $r = \sin\alpha$, using formula 11.4.10. from Abramowitz Stegun and the equality

$$J_{3/2}(x) = \sqrt{\frac{2}{\pi}}\frac{\sin x - x\cos x}{x^{3/2}},$$

we have :

$$\widehat{B^s}(\rho,0) = B_0^s\int_0^1 \sqrt{1-r^2}J_0(\rho r)\ r\ \mathrm{d}r \tag{A.4}$$

$$= B_0^s\int_0^{\pi/2}\cos^2\alpha\sin\alpha\ J_0(\rho\sin\alpha)\mathrm{d}\alpha \tag{A.5}$$

$$= B_0^s\sqrt{2}\ \Gamma\left(\frac{3}{2}\right)\frac{J_{3/2}(\rho)}{\rho^{3/2}} \tag{A.6}$$

$$= B_0^s\sqrt{\frac{\pi}{2}}\ \frac{J_{3/2}(\rho)}{\rho^{3/2}} \tag{A.7}$$

$$\widehat{B^s}(\rho,0) = B_0^s\frac{\sin\rho - \rho\cos\rho}{\rho^3} \tag{A.8}$$

And similarly for

$$\widehat{B^b}(\rho,0) = B_0^b\frac{\sin\rho - \rho\cos\rho}{\rho^3} \tag{A.9}$$

From these identities,the steady state streamfunction at the two levels are :

$$\Psi^s(r,\phi,z=0,t) = \int_0^\infty \frac{J_0(\rho r)}{\sigma\sinh(\rho\sigma)} \frac{\sin\rho - \rho\cos\rho}{\rho^3} \left(B_0^b - B_0^s\cosh(\rho\sigma)\right) \mathrm{d}\rho \tag{A.10a}$$

$$\Psi^b(r,\phi,z=1,t) = \int_0^\infty \frac{J_0(\rho r)}{\sigma\sinh(\rho\sigma)} \frac{\sin\rho - \rho\cos\rho}{\rho^3} \left(B_0^b\cosh(\rho\sigma) - B_0^s\right) \mathrm{d}\rho \tag{A.10b}$$

The steady state velocity field : the radial velocities are null because the streamfunctions have no angular component and $U_\phi = \dfrac{\mathrm{d}\Psi}{\mathrm{d}r}$ so :

$$U_\phi^s = B_0^b E(r,\sigma) + B_0^s F(r,\sigma) \tag{A.11a}$$

$$U_\phi^b = B_0^b F(r,\sigma) + B_0^s E(r,\sigma) \tag{A.11b}$$

where the function E and F are defined by the following integrals :

$$E(r,\sigma) = \int_0^\infty \frac{J_1(\rho r)}{\sigma\sinh(\rho\sigma)} \frac{\rho\cos\rho - \sin\rho}{\rho^2} \mathrm{d}\rho \tag{A.12a}$$

$$F(r,\sigma) = \int_0^\infty \frac{J_1(\rho r)}{\sigma\tanh(\rho\sigma)} \frac{\rho\cos\rho - \sin\rho}{\rho^2} \mathrm{d}\rho \tag{A.12b}$$

References

Badin, G. and Poulin, F.J., Asymptotic scale-dependent stability of surface quasi-geostrophic vortices: semi-analytic results. *Geophysical & Astrophysical Fluid Dynamics*, 2019, **113**, 574–593.

Baey, J.M. and Carton, X., Vortex multipoles in two-layer rotating shallow-water flows. *Journal of Fluid Mechanics*, 2002, pp. 151–175.

Bosse, A., Testor, P., Houpert, L., Damien, P., Prieur, L., Hayes, D., Taillandier, V., Durrieu de Madron, X., d'Ortenzio, F., Coppola, L., Karstensen, J. and Mortier, L., Scales and dynamics of Submesoscale Coherent Vortices formed by deep convection in the northwestern Mediterranean Sea. *Journal of Geophysical Research: Oceans*, 2016, **121**, 7716–7742.

Bretherton, F.P., Critical layer instability in baroclinic flows. *Quarterly Journal of the Royal Meteorological Society*, 1966, **92**, 325–334.

Carton, X., Instability of Surface Quasigeostrophic Vortices. *Journal of the Atmospheric Sciences*, 2009, **66**, 1051–1062.

Carton, X., Flierl, G.R., Perrot, X., Meunier, T. and Sokolovskiy, M.A., Explosive instability of geostrophic vortices. Part 1: baroclinic instability. *Theoretical and computational fluid dynamics*, 2010, **24**, 125–130.

Carton, X.J., Hydrodynamical modelling of oceanic vortices. *Surveys in Geophysics*, 2001, **22**, 179–263.

Carton, X.J., Oceanic Vortices; in *Fronts, Waves and Vortices in Geophysical Flows*, edited by J.B. Flor, Vol. Lecture Notes in Physics, 805, 2010, pp. 61–108.

Carton, X.J. and McWilliams, J.C., Nonlinear oscillatory evolution of a baroclinically unstable geostrophic vortex. *Dynamics of Atmospheres and Oceans*, 1996, pp. 207–214.

Carton, X.J., Poulin, F.P. and Pavec, M., Linear baroclinic and parametric instabilities of boundary currents. *Geophysical and Astrophysical Fluid Dynamics*, 2011, **105**, 453–477.

Charney, J.G., On the scale of atmospheric motions. *Geofys. Publikasjoner*, 1948, pp. 1–17.

Chavanne, C., Flament, P. and Gurgel, K.W., Interactions between a Submesoscale Anticyclonic Vortex and a Front. *Journal of Physical Oceanography*, 2010, **40**.

Dritschel, D.G., An exact, steadily rotating surface quasi-geostrophic elliptical vortex. *Geophysical and Astrophysical Fluid Dynamics*, 2011, **105**, 368–376.

Eady, E.T., Long Waves and Cyclone Waves. *Tellus*, 1949, **1**, 33–52.

Flierl, G.R., Models of vertical structure and the calibration of two-layer models. *Dynamics of Atmospheres and Oceans*, 1978, **2**, 341–381.

Flierl, G.R., On the instability of geostrophic vortices. *Journal of Fluid Mechanics*, 1988, pp. 349–388.

Gryanik, V.M., Dynamics of singular geostrophic vortices in a two-level model of the atmosphere (or ocean). *Izvestiya Akademia Nauk. SSSR, Atmospheric and Oceanic Physics*, 1983, **19**, 171–179.

Gula, J., Molemaker, M.J. and McWilliams, J.C., Topographic vorticity generation, submesoscale instability and vortex street formation in the Gulf Stream. *Geophysical Research Letters*, 2015, **42**, 4054–4062.

Gula, J., Blacic, T.M. and Todd, R.E., Submesoscale Coherent Vortices in the Gulf Stream. *Geophysical Research Letters*, 2019, **46**, 1–11.

Gula, J., Taylor, J., Scherbina, A. and Mahadevan, A., Submesoscale processes and mixing; in *Ocean Mixing*, Vol. chapter 8, 2022, pp. 181–214.

Harvey, B.J. and Ambaum, M.H.P., Perturbed Rankine vortices in surface quasi-geostrophic dynamics. *Geophysical & Astrophysical Fluid Dynamics*, 2011, **105**, 377–391.

Harvey, B.J., Ambaum, M.H.P. and Carton, X., Instability of shielded surface temperature vortices. *Journal of the Atmospheric Sciences*, 2011, **68**, 964–971.

Held, I., PierreHumbert, R.T., Garner, S.T. and Swanson, K.L., Surface quasi-geostrophic dynamics. *Journal of Fluid Mechanics*, 1995, pp. 1–20.

Helfrich, K. and Send, U., Finite-amplitude evolution of two-layer geostrophic vortices. *Journal of Fluid Mechanics*, 1988, pp. 331–348.

Hogg, N.G. and M., S.H., The heton, an elementary interaction between discrete baroclinic geostrophic vortices, and its implications concerning eddy heat-flow. *Proceedings of the Royal Society London A*, 1985a, **397**, 1–20.

Hogg, N.G. and M., S.H., Hetonic Explosions: The Breakup and Spread of Warm Pools as Explained by Baroclinic Point Vortices. *Journal of the Atmospheric Sciences*, 1985b, **42**, 1465–1476.

Hopfinger, E.J. and van Heijst, G.J.F., Vortices in rotating fluids. *Annual Review of Fluid Mechanics*, 1993, **25**, 241–289.

Klein, P., Hua, B.L., Lapeyre, G., Capet, X., Le Gentil, S. and Sasaki, H., Upper Ocean Turbulence from High-Resolution 3D Simulations. *Journal of Physical Oceanography*, 2008, **38**, 1748–1763.

Lapeyre, G. and Klein, P., Dynamics of the Upper Oceanic Layers in Terms of Surface Quasigeostrophy Theory. *Journal of Physical Oceanography*, 2006, **36**, 165–176.

Lapeyre, G., Surface Quasi-Geostrophy. *Fluids*, 2017, **2**, 1–28.

McWilliams, J.C., Submesoscale, coherent vortices in the ocean. *Reviews of Geophysics*, 1985, **23**, 165–182.

McWilliams, J.C., Geostrophic Vortices; in , 1991, pp. 5–50.

Melander, M.V., Zabusky, N.J. and McWilliams, J.C., Symmetric vortex merger in two dimensions - Causes and conditions. *Journal of Fluid Mechanics*, 1988, **195**, 303–340.

Morvan, M., L'Hégaret, P., Carton, X., Gula, J., Vic, C., de Marez, C., Sokolovskiy, M. and Koshel, K., The life cycle of submesoscale eddies generated by topographic interactions. *Ocean Science*, 2019, **15**, 1531–1543.

Oulhen, E., Reinaud, J. and Carton, X., Formation of small scale vortices in the core of a large merged vortex. *Geophysical and Astrophysical Fluid Dynamics*, 2022, **116**, 411–432.

Perrot, X., Reinaud, J., Carton, X. and Dritschel, D., Homostrophic vortex interaction in a coupled QG-SQG model. *Regular and Chaotic Dynamics*, 2010, **15**, 67–84.

Phillips, N.A., Energy Transformations and Meridional Circulations associated with simple Baroclinic Waves in a two-level, Quasi-geostrophic Model. *Tellus*, 1954, **6**, 274–286.

Polvani, L., Two-layer geostrophic vortex dynamics. Part 2. Alignment and two-layer V-states. *Journal of Fluid Mechanics*, 1991, **225**, 241–270.

Polvani, L.M., Zabusky, N.J. and Flierl, G.R., Two-layer geostrophic vortex dynamics. Part 1. Upper-layer V-states and merger. *Journal of Fluid Mechanics*, 1989, **205**, 215–242.

Provenzale, A., Transport by coherent barotropic vortices. *Annual Review of Fluid Mechanics*, 1999, **31**, 55–93.

Reinaud, J., Three-dimensional quasi-geostrophic vortex equilibria with m-fold symmetry. *Journal of Fluid Mechanics*, 2019, **863**, 32–59.

Reinaud, J.N. and Carton, X.J., Existence, stability and formation of baroclinic tripoles in quasi-geostrophic flows. *Journal of Fluid Mechanics*, 2009a, **785**, 1–30.

Reinaud, J.N. and Carton, X.J., The stability and the nonlinear evolution of quasi-geostrophic hetons. *Journal of Fluid Mechanics*, 2009b, **636**, 109–135.

Reinaud, J.N., Dritschel, D.G. and Scott, R.K., Self-similar collapse of three vortices in the generalised Euler and quasi-geostrophic equations. *Physica D: Nonlinear Phenomena*, 2022, **434**.

Reinaud, J., Dritschel, D. and Carton, X., Interaction between a surface quasi-geostrophic buoyancy anomaly strip and an internal vortex. *Geophysical and Astrophysical Fluid Dynamics*, 2016, **110**, 461–490.

Reinaud, J., Dritschel, D. and Carton, X., Interaction between a quasi-geostrophic buoyancy filament and a heton. *Fluids*, 2017a, **2**, 37.

Reinaud, J., Dritschel, D. and Carton, X., Interaction between a surface quasi-geostrophic buoyancy anomaly jet and internal vortices. *Physics of Fluids*, 2017b, **29**.

Richardson, P.L., Gulf-Stream rings; in *Eddies in Marine Science*, edited by A.R. Robinson, Vol. Topics in Atmospheric and Oceanographic Sciences, 1983, pp. 19–45.

Robinson, A.R., *Eddies in Marine Science*, 2012 (Springer).

Smith, K.S. and Bernard, E., Geostrophic turbulence near rapid changes in stratification. *Physics of Fluids*, 2013, **25**, 046601.

Sokolovskiy, M.A. and Carton, X.J., Baroclinic multipole formation from heton interaction. *Fluid Dynamics Research*, 2010, pp. –.

Sokolovskiy, M.A. and Verron, J., *Dynamics of Vortex Structures in a Stratified Rotating Fluid*, 2013 (Spriger).

Tulloch, R. and Smith, K.S., Quasigeostrophic Turbulence with Explicit Surface Dynamics: Application to the Atmospheric Energy Spectrum. *Journal of the Atmospheric Sciences*, 2009, **66**, 450–467.

van Heijst, G.J.F., Dynamics of vortices in rotating and stratified fluids; in *Fronts, waves and vortices in geophysical flows*, 2010, pp. 1–33.

Vic, A., Carton, X. and Gula, J., Eady baroclinic instability of a circular vortex. *Symmetry*, 2022, **14**, 1–18.

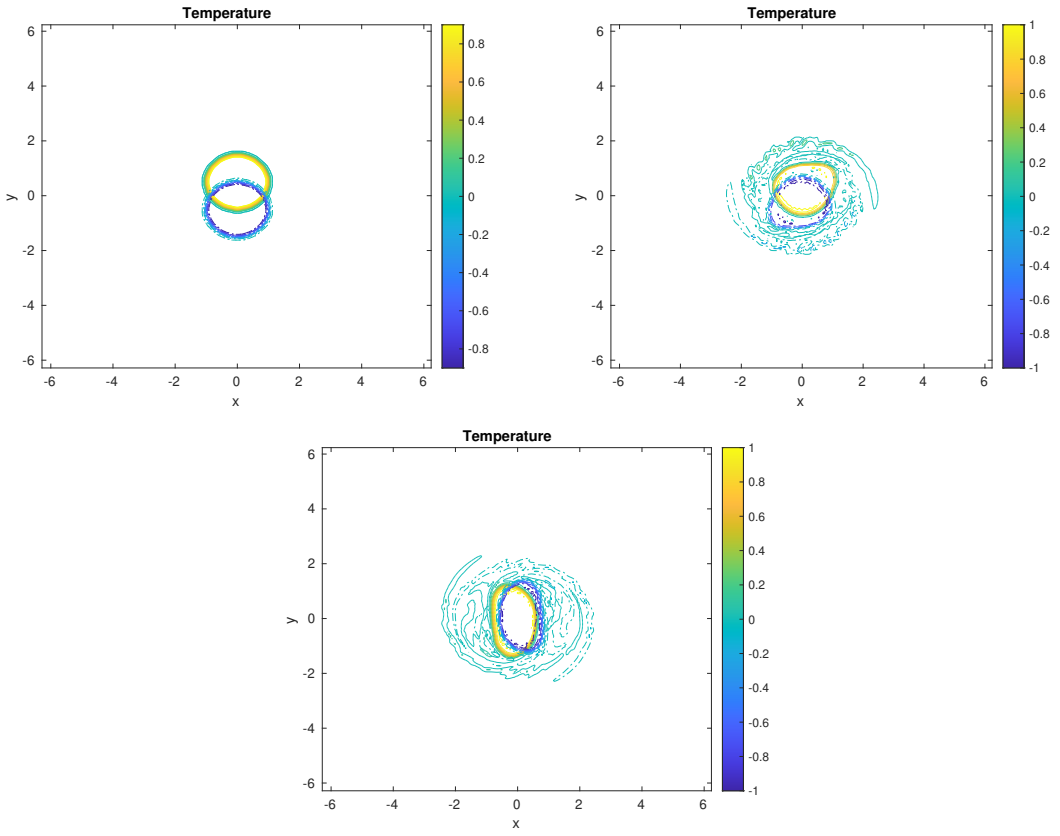

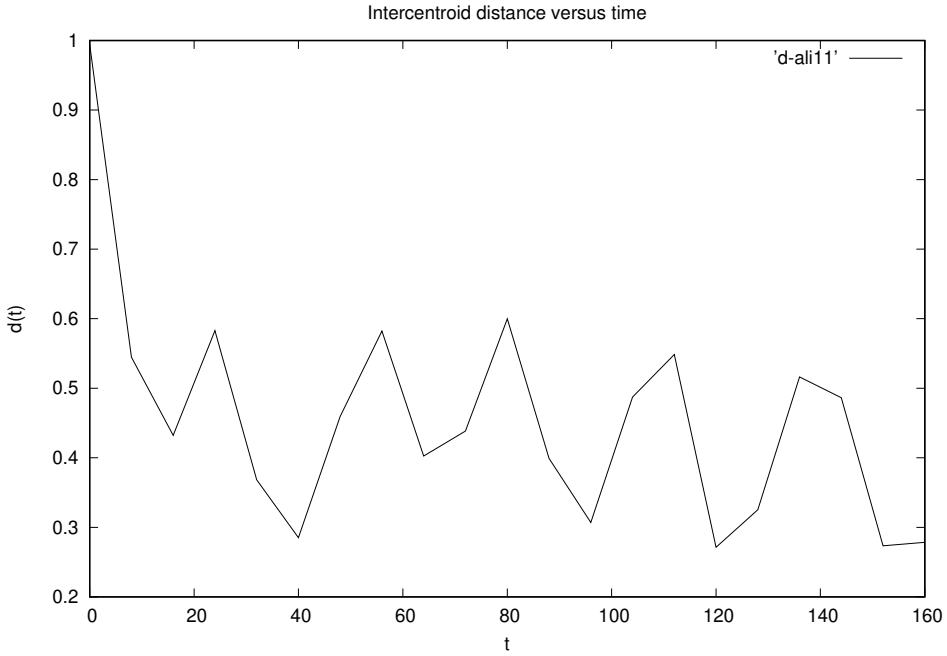

Figure 11. (Top and middle) Time series of buoyancy maps for the upper level (solid lines) and the lower level (dashed lines) superimposed, showing the evolution of a tilted vortex towards a vertical column. Times shown are t=0, 24, 40 model time units. The vortex parameters are $B_1 = 1, B_2 = -1.0$, $R_1 = R_2 = 1.0$, $H = R_d = 1$, $d = 1$; (bottom) Time series of the inter-centroid distance for this simulation.

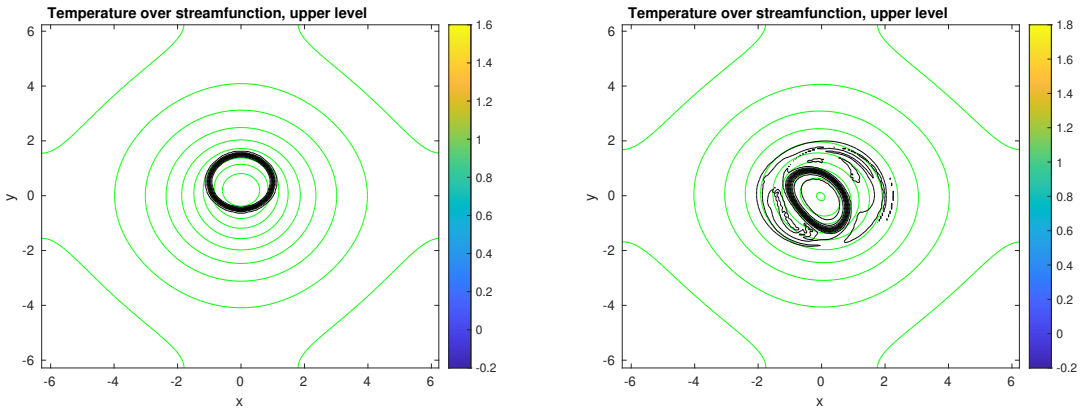

Figure 12. Maps of buoyancy (black dashed lines) superimposed on streamlines (green solid lines) for the upper level. Times shown are t=0, model time units. The vortex parameters are $B_1 = 1, B_2 = -1.0$, $R_1 = R_2 = 1.0$, $H = R_d = 1$, $d = 1$.

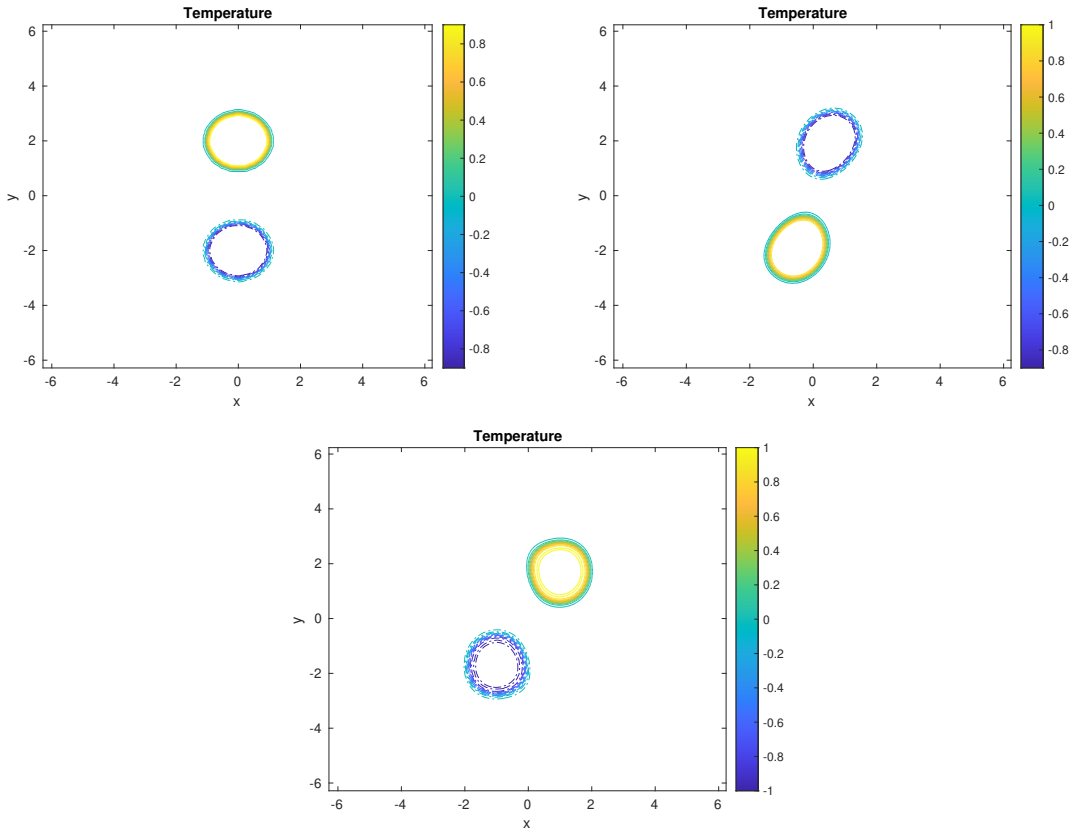

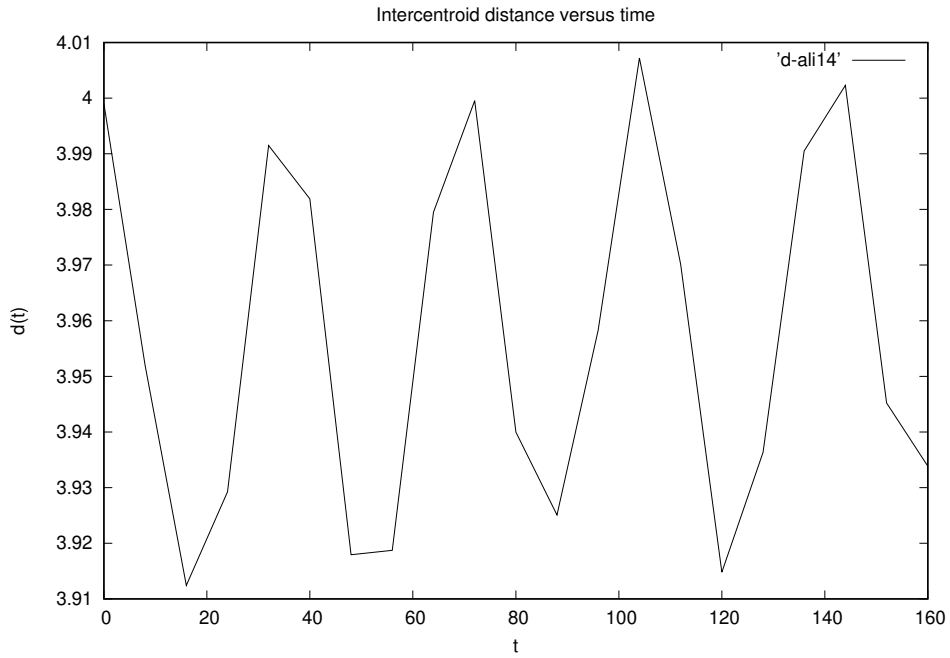

Figure 13. (Top and middle) Time series of buoyancy maps for the upper level (solid lines) and the lower level (dashed lines) superimposed, showing the co-rotation of a tilted vortex around the plane center. Times shown are t=0, 64, 128 model time units. The vortex parameters are $B_1 = 1, B_2 = -1.0$, $R_1 = R_2 = 1.0$, $H = R_d = 1$, $d = 4$; (bottom) Time series of the inter-centroid distance for this simulation.

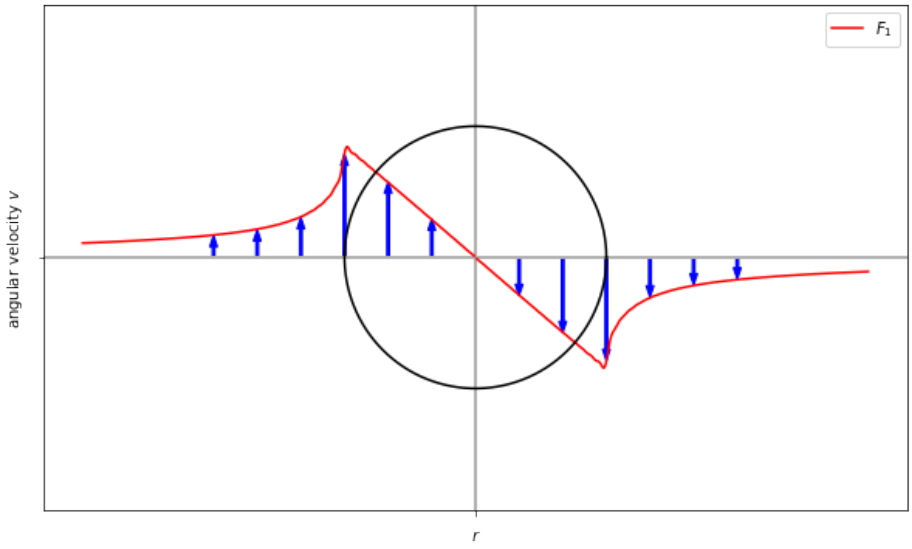

Figure A1. Graphs of the angular velocity

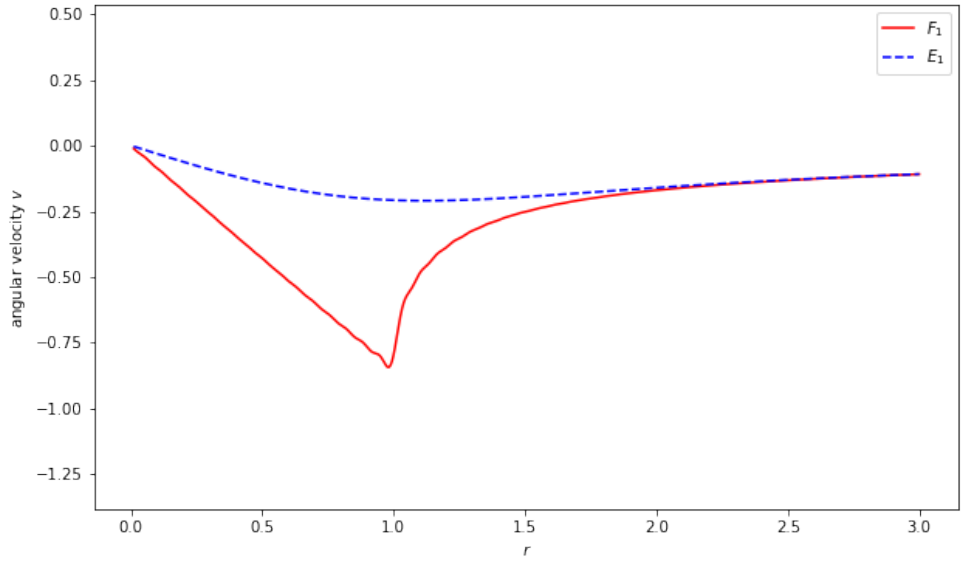

Figure A2. Graphs of the function E and F for fixed $\sigma = 1$